

An ab-initio study of circular photogalvanic effect in chiral multifold semimetals

Congcong Le,¹ Yang Zhang,² Claudia Felser,^{1,3} and Yan Sun^{1,*}

¹Max Planck Institute for Chemical Physics of Solids, 01187 Dresden, Germany

²Department of Physics, Massachusetts Institute of Technology, Cambridge, Massachusetts 02139, USA

³Oxford Street, LISE 308 Cambridge, Massachusetts 02138, USA

(Dated: May 26, 2020)

So far, the circular photogalvanic effect (CPGE) is the only possible quantized signal in Weyl semimetals. With inversion and mirror symmetries broken, Weyl and multifold fermions in band structures with opposite chiralities can stay at different energies and generate a net topological charge. Such kind of net topological charge can present as a quantized signal in the circular polarized light induced injection current. According to current theoretical understanding, RhSi and its counterparts are believed to be the most promising candidate for the experimental observation of the quantized CPGE. However, the real quantized signal was not experimentally observed to date. Since all the previous theoretical studies for the quantized CPGE were based on effective model but not realistic band structures, it should lose some crucial details that influence the quantized signal. The current status motives us to perform a realistic ab-initio study for the CPGE. Our result shows that the quantized value is very easy to be interfered by trivial bands related optic transitions, and an fine tuning of the chemical potential by doping is essential for the observation of quantized CPGE. This work performs the first ab-initio analysis for the quantized CPGE based on realistic electronic band structure and provides an effective way to solve the current problem for given materials.

PACS numbers: 75.85.+t, 75.10.Hk, 71.70.Ej, 71.15.Mb

I. INTRODUCTION

The band crossings with nontrivial topological invariant, including Weyl, Dirac and unconventional fermions, have been attracting enormous attention in condensed matter¹⁻³. For Weyl and Dirac fermions⁴⁻¹⁸, they were realized experimentally in the topological semimetal materials and further classified into the type-I and type-II classes¹⁹. Unconventional fermions, which contain three-, four-, six- and eightfold degenerate points, are exhaustively classified by space group symmetries in solid-state systems with spin-orbit coupling and time-reversal symmetry. These multifold degenerate points with nontrivial topological numbers lead to a series of exotic effects such as surface Fermi arcs^{4,5}, the chiral anomaly^{20,21}, large anomalous Hall and spin Hall effect²²⁻²⁴ and circular photogalvanic effects²⁵⁻³⁰.

Recently, it has been pointed out^{29,30} that a single multifold degenerate point with nontrivial invariant can lead to quantized CPGE trace, which can directly measure the topological charge of degenerate points. So far it is the only quantized signal exists in topological semimetals. Those topological degenerate points in solid-state systems always obey the Nielsen-Ninomiya Theorem as the ground rule³¹⁻³³. A topological degenerate point inevitably accompanies another topological point with opposite charge, because the total charges in the entire BZ must be neutralized. If all degenerate points with opposite charges are the same energy due to crystal symmetries, the total CPGE trace contributed to all degenerate points is zero. In the time-reversal and crystal symmetries, only inversion and mirror symmetries can change the charge sign of degenerate points, indicating that the degenerate points with opposite charges have the same energy for the system with inversion and mirror symmetries. Therefore, the non-magnetic chiral topological semimetal materials with chiral space group, only including time-reversal and rotational sym-

metries, have different energy for degenerate points with opposite charge and can come true quantized CPGE trace due to Pauli blocking.

In the chiral topological semimetal materials, RhSi is the most promising candidate to exhibit quantized CPGE trace. There are two reasons: the multifold degenerate points and exotic Fermi arcs were confirmed by ARPES measurements³⁴; A big energy difference between fourfold and sixfold points exist, which is beneficial to acquire quantized CPGE trace due to Pauli blocking^{30,35,36}. Hence, RhSi gets extensive attentions in experiments. However, theoretically predicted the quantized CPGE^{30,35} is not observed in experiments³⁷. We notice that all the previous theoretical studies for quantized CPGE are based on few bands effective $k \cdot p$ and tight binding models with only considering the bands near degenerated points. Since the second order optical response is very sensitive to the details of bands, such kind of approximation is easy to loss some crucial information that influence the quantized signal. The current situation motive us to perform an ab-initio analysis for the CPGE in RhSi based on realistic electronic band structure by first principle calculations.

The paper is organized as follows. In Section. II, the symmetry analysis of CPGE tensor in chiral topological semimetal RhSi is presented. Then, in Section. III, the difference of CPGE trace between effective model and real materials are summarized. In Section. IV, we discuss CPGE trace in RhSi and other related compounds(CoSi, PdGa, PtGa, PtAl, RhSn). Finally, in Section. V, we give a summary of our paper.

II. SYMMETRY ANALYSIS OF CPGE TENSOR

The CPGE injection current and CPGE tensor β can be written as^{29,38}

$$\frac{dj_i}{dt} = \beta_{ij}(\omega) \left[\vec{E}(\omega) \times \vec{E}^*(\omega) \right]_j,$$

$$\beta_{ij}(\omega) = \frac{\pi e^3}{\hbar^2 V} \sum_{\vec{k}, n, m} f_{nm}^{\vec{k}} \Delta_{\vec{k}, nm}^i R_{\vec{k}, nm}^j \delta(\hbar\omega - E_{\vec{k}, mn}) \quad (1)$$

Where $\vec{E}^*(\omega) = \vec{E}(-\omega)$ is the electric field of circularly polarized light, and i and j index are the direction of current and circular polarized light respectively. $R_{\vec{k}, nm}^j = \epsilon_{jkl} r_{\vec{k}, nm}^k r_{\vec{k}, mn}^l$, $E_{\vec{k}, mn} = E_{\vec{k}, m} - E_{\vec{k}, n}$ and $f_{nm}^{\vec{k}} = f_n^{\vec{k}} - f_m^{\vec{k}}$ are difference between band energies and Fermi-Dirac distributions, $\Delta_{\vec{k}, nm}^i = \partial_{k_i} E(\vec{k})_{nm}$, and $r_{\vec{k}, nm}^i = i \langle m(\vec{k}) | \partial_{k_i} | n(\vec{k}) \rangle$.

The relation of $\Delta_{\vec{k}, nm}^i$, $R_{\vec{k}, nm}^i$ and $r_{\vec{k}, nm}^i$ between \vec{k} and $g\vec{k}$ is given by

$$\Delta_{g\vec{k}, nm}^i = \frac{\partial E_{nm}(g\vec{k})}{\partial k_i} = \sum_{i'} \frac{\partial (g\vec{k})_{i'}}{\partial k_i} \Delta_{\vec{k}, nm}^{i'}$$

$$r_{g\vec{k}, nm}^i = i \langle m(g\vec{k}) | \frac{\partial}{\partial k_i} | n(g\vec{k}) \rangle = \sum_{i'} \frac{\partial (g\vec{k})_{i'}}{\partial k_i} r_{\vec{k}, nm}^{i'}$$

$$R_{g\vec{k}, nm}^i = \epsilon_{ikl} \left[\sum_{k'} \frac{\partial (g\vec{k})_{k'}}{\partial k_k} r_{\vec{k}, nm}^{k'} \right] \left[\sum_{l'} \frac{\partial (g\vec{k})_{l'}}{\partial k_l} r_{\vec{k}, nm}^{l'} \right],$$

$$= \epsilon_{ikl} \sum_{k', l'} \frac{\partial (g\vec{k})_{k'}}{\partial k_k} \frac{\partial (g\vec{k})_{l'}}{\partial k_l} r_{\vec{k}, nm}^{k'} r_{\vec{k}, nm}^{l'},$$

$$= \epsilon_{ikl} \sum_{k', l'} \frac{\partial (g\vec{k})_{k'}}{\partial k_k} \frac{\partial (g\vec{k})_{l'}}{\partial k_l} \epsilon_{i'k'l'} \epsilon_{i'k'l'} r_{\vec{k}, nm}^{k'} r_{\vec{k}, nm}^{l'},$$

$$= \epsilon_{ikl} \sum_{k', l'} \frac{\partial (g\vec{k})_{k'}}{\partial k_k} \frac{\partial (g\vec{k})_{l'}}{\partial k_l} \epsilon_{i'k'l'} R_{\vec{k}, nm}^{i'} \quad (2)$$

Then, we consider the relation of $\beta_{ij}(\vec{k}, \omega)$ and $\beta_{ij}(g\vec{k}, \omega)$ connected by crystal symmetry g , which is given by

$$\beta_{ij}(g\vec{k}, \omega),$$

$$= \frac{\pi e^3}{\hbar V} \sum_{k, n, m} f_{nm}^{g\vec{k}} \Delta_{g\vec{k}, nm}^i R_{g\vec{k}, nm}^j \delta(\hbar\omega - E_{g\vec{k}, mn}),$$

$$= \frac{\pi e^3}{\hbar V} \epsilon_{ikl} \sum_{\vec{k}, n, m} f_{nm}^{\vec{k}} \left[\sum_{i'} \frac{\partial (g\vec{k})_{i'}}{\partial k_i} \Delta_{\vec{k}, nm}^{i'} \right]$$

$$\left[\sum_{k', l'} \frac{\partial (g\vec{k})_{k'}}{\partial k_k} \frac{\partial (g\vec{k})_{l'}}{\partial k_l} \epsilon_{j'k'l'} R_{\vec{k}, nm}^{j'} \right] \delta(\hbar\omega - E_{\vec{k}, mn})$$

$$= \sum_{i', k', l'} \frac{\partial (g\vec{k})_{i'}}{\partial k_i} \frac{\partial (g\vec{k})_{k'}}{\partial k_k} \frac{\partial (g\vec{k})_{l'}}{\partial k_l} \epsilon_{j'k'l'} \epsilon_{ikl} \beta_{i'j'}(\vec{k}, \omega) \quad (3)$$

Hence, the nonsymmorphic symmetries, which are screw axis only in RhSi, have the same as symmorphic symme-

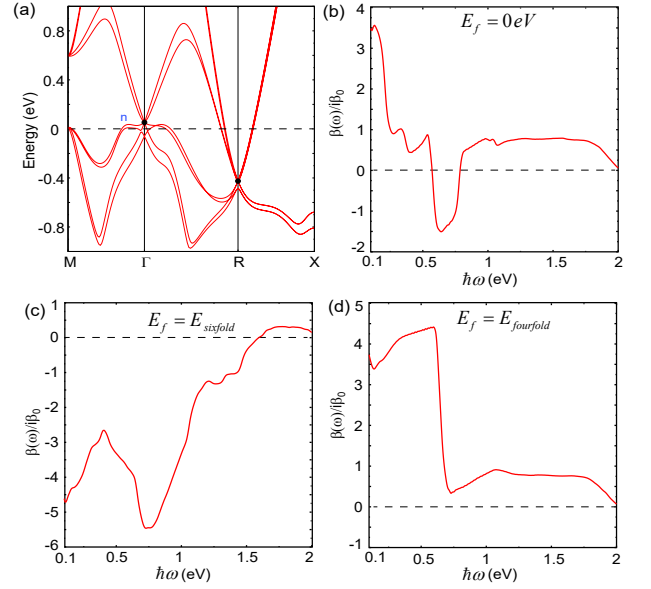


FIG. 1: (color online) (a) band structure of RhSi with SOC in the paramagnetic state; black points denote fourfold and sixfold degenerate points at Γ and M points, and the numbers n with blue color represent a band number of four degenerate points. (b)-(d) show trace of the CPGE tensor as a function of frequency $\hbar\omega$ by DFT calculations with corresponding Fermi level $E_f = 0$ eV, $E_{sixfold}$, $E_{fourfold}$, respectively.

tries for the CPGE tensor. It is clear that the CPGE tensor $\beta_{ij}(\omega)$ of system with inversion symmetry is zero due to $\beta_{ij}(\vec{k}, \omega) = -\beta_{ij}(-\vec{k}, \omega)$, and the materials with non-zero CPGE tensor should belong to the gyrotropic point groups without inversion.

The crystal structure of RhSi has nonsymmorphic space group $G=P2_13$ (No.198), and the quotient group G/Γ is specified by 12 symmetry operations, where we denote T as the translation group with respect to the unit cell. In 16 symmetry operations, nonsymmorphic symmetry operations are $\tilde{C}_{2x} = \{C_{2x}|1/2, 1/2, 0\}$, $\tilde{C}_{2y} = \{C_{2y}|0, 1/2, 1/2\}$, and $\tilde{C}_{2z} = \{C_{2z}|1/2, 0, 1/2\}$. Under crystal symmetries $g = C_{2x/y/z}$, the relation of $\beta_{ij}(\vec{k}, \omega)$ and $\beta_{ij}(g\vec{k}, \omega)$ can be written as

$$\beta_{ii}(g\vec{k}, \omega) = \beta_{ii}(\vec{k}, \omega) \quad (i = j)$$

$$\beta_{ij}(g\vec{k}, \omega) = -\beta_{ij}(\vec{k}, \omega) \quad (i \neq j) \quad (4)$$

Due to $C_{2x/y/z}$ rotational symmetries, $\beta_{ij}(\omega)$ ($i \neq j$) is zero and $\beta_{ii}(\omega)$ is non-zero. We will focus on diagonal CPGE tensor $\beta_{ii}(\omega)$. Under crystal symmetries $g = C_{3,111}$, the relation of $\beta_{ij}(\vec{k}, \omega)$ and $\beta_{ij}(g\vec{k}, \omega)$ can be given by

$$\beta_{xx}(\vec{k}, \omega) = \beta_{zz}(C_{3,111}\vec{k}, \omega), \quad \beta_{yy}(\vec{k}, \omega) = \beta_{xx}(C_{3,111}\vec{k}, \omega),$$

$$\beta_{zz}(\vec{k}, \omega) = \beta_{yy}(C_{3,111}\vec{k}, \omega) \quad (5)$$

III. DIFFERENCE BETWEEN EFFECTIVE MODEL AND REAL MATERIALS

From the effective models for multifold degenerate points with linear dispersion, the exact quantization of the CPGE trace is predicted in a certain frequency range^{29,30}. The following is a brief summary of derivation about quantized CPGE trace^{29,30}. The CPGE trace can be rewritten as

$$\beta(\omega) = \frac{4\pi^2\beta_0}{V} \sum_{\vec{k}, i, n, m} f_{nm}^{\vec{k}} \Delta_{\vec{k}, nm}^i R_{\vec{k}, nm}^i \delta(\hbar\omega - E_{\vec{k}, mn}) \quad (6)$$

Where $\beta_0 = \frac{\pi e^3}{h^2}$, and the relation between $\vec{R}_{\vec{k}, nm}$ and Berry curvature is $\vec{\Omega}_{\vec{k}, n} = i \sum_{m \neq n} \vec{R}_{\vec{k}, nm}$.

The topological property of degenerate points can be characterized by the Chern number

$$C_n = \frac{1}{2\pi} \oint_S \vec{\Omega}_n(\vec{k}) \cdot d\vec{S}_n \quad (7)$$

Where \vec{S}_n is a closed surface of band n enclosing the degenerate points, and $\vec{\Omega}_n(\vec{k}) = \nabla_{\vec{k}} \times \langle \psi_n(\vec{k}) | i \nabla_{\vec{k}} | \psi_n(\vec{k}) \rangle$ is the Berry curvature of band n .

In spherical coordinates, The CPGE trace becomes

$$\begin{aligned} \beta(\omega) &= 4\pi^2\beta_0 \sum_{i, k, n, m} \int \frac{k^2 dk d\Omega}{(2\pi)^3} \partial_{\vec{k}} E_{\vec{k}, nm} \cdot \vec{R}_{\vec{k}, nm} \delta(\hbar\omega - E_{\vec{k}, mn}) \\ &= 4\pi^2\beta_0 \sum_{n, m} \int \frac{k^2 dk d\Omega}{(2\pi)^3} \partial_{\vec{k}} E_{\vec{k}, nm}^{\hat{k}} R_{\vec{k}, nm}^{\hat{k}} \delta(\hbar\omega - E_{\vec{k}, mn}) \\ &= 4\pi^2\beta_0 \sum_{n, m} \int \frac{d(E_{k, nm}) d\Omega}{(2\pi)^3} k^2 R_{k, nm}^{\hat{k}} \delta(\hbar\omega - E_{\vec{k}, mn}) \\ &= 4\pi^2\beta_0 \sum_{n, m} \int \frac{d\Omega}{(2\pi)^3} k^2 (\hbar\omega) R_{nm}^{\hat{k}}(\hbar\omega) \\ &= 4\pi^2\beta_0 \sum_{n, m} \int dS_{nm}^{\hat{k}} R_{nm}^{\hat{k}}, \\ &= 4\pi^2\beta_0 \sum_{n, m} \int d\vec{S}_{nm} \cdot \vec{R}_{nm} \end{aligned} \quad (8)$$

Where $\partial_{\vec{k}} E_{\vec{k}, nm} = \partial_k E_{k, nm}^{\hat{k}} \hat{k} + \frac{1}{k} \partial_{\theta} E_{k, nm}^{\hat{\theta}} \hat{\theta} + \frac{1}{k \sin \theta} \partial_{\phi} E_{k, nm}^{\hat{\phi}} \hat{\phi}$ and $\vec{R}_{\vec{k}, nm} = R_{k, nm}^{\hat{k}} \hat{k} + R_{k, nm}^{\hat{\theta}} \hat{\theta} + R_{k, nm}^{\hat{\phi}} \hat{\phi}$, \vec{R}_{nm} has only the radial component in spherical coordinates for multifold degenerate points with linear dispersion. For a given frequency ω , the delta function and Fermi-Dirac distributions select a surface \vec{S}_{nm} in the \vec{k} space where $E_{\vec{k}, nm} = \hbar\omega$, and $d\vec{S}$ denotes the oriented surface element normal to \vec{S} . Hence the CPGE trace is physically understood as the Berry flux penetrating through \vec{S} . For a single type-I Weyl point, when the Fermi level is located at the Weyl point, the CPGE

trace is $\beta(\omega) = iC\beta_0$ where C is Chern number of the occupied band. Similar to type-I Weyl points, other multifold fermions can also obtain quantized CPGE trace according to the above derivation.

The above results are based on the effective $k \cdot p$ models of multifold fermions. However, for real nonmagnetic chiral topological semimetal materials, there are some factors that affect quantized CPGE trace:

(1) Except for the bands that form the degenerate points, there are many extra bands in real materials, which can induce corrections of relation between \vec{R} and $\vec{\Omega}_n$ compared with that of the effective model.

(2) The condition for quantization is that the band structures near multifold fermion have linear dispersion, indicating that higher-order band dispersions can modify the CPGE trace.

(3) The nontrivial band structures that form multifold fermions can contribute quantized CPGE trace, while other trivial band structures are allowed optical transitions and can provide CPGE.

IV. AB INITIO ANALYSIS OF CIRCULAR PHOTO GALVANIC EFFECT (CPGE)

To calculate CPGE tensor, we project the *ab-initio* DFT Bloch wave function into high symmetric atomic-orbital-like Wannier functions³⁹ with diagonal position operator, as performed in the code of the full-potential local-orbital minimum-basis (FPLO)^{40,41}. For obtaining precise Wannier functions, we include the most outside d-, s-, and p-orbital for Rh, most outside s- and p-orbital for element Si, which guarantees the full bands overlap from *ab-initio* and Wannier functions in the energy window from -10 to 10 eV. With highly symmetric Wannier functions, we construct an effective tight-binding model Hamiltonian and calculate the photoconductivity by the Eqs. 1.

Fig.1(a) shows the band structure of RhSi with spin-orbital coupling (SOC) in the paramagnetic state. Near the Fermi level, the valence and conduction bands are mainly attributed to the Rh-4d orbitals. A fourfold degeneracy at Γ points with the energy $E_{fourfold}=50$ meV is protected by point group T and time-reversal symmetry, which can be understood by the character tables of point group T. A sixfold degeneracy at R points with the energy $E_{sixfold}=400$ meV is protected by non-symmorphic symmetries ($\{C_{3,111}^{-1} | 010\}$, $\{C_{2x} | \frac{1}{2} \frac{3}{2} 0\}$ and $\{C_{2y} | 0 \frac{3}{2} \frac{3}{2}\}$) and time-reversal symmetry³. Because degeneracy points at Γ and R are not symmetrically related, the energies of these points can be different. The fourfold degeneracy at Γ point is described a spin-3/2 fermion with Chern number $C=3, 1, -1, -3$ for four bands^{35,36}, and the sixfold degeneracy at R point is double spin-1 fermion with $C=2, 2, 0, 0, -2, -2$ for six bands, which satisfies Nielsen-Ninomiya theorem³¹⁻³³.

We firstly calculated the trace of CPGE tensor with Fermi level lying at the charge neutral points, which should close to the case in experimental measurements³⁷. As presented in Fig.1(b), one can see any quantized value in the long rang of frequency from 0.1 to 2.0 eV, and the plateau close to $4\beta_0$ is absent, which consists with experimental results³⁷. For ex-

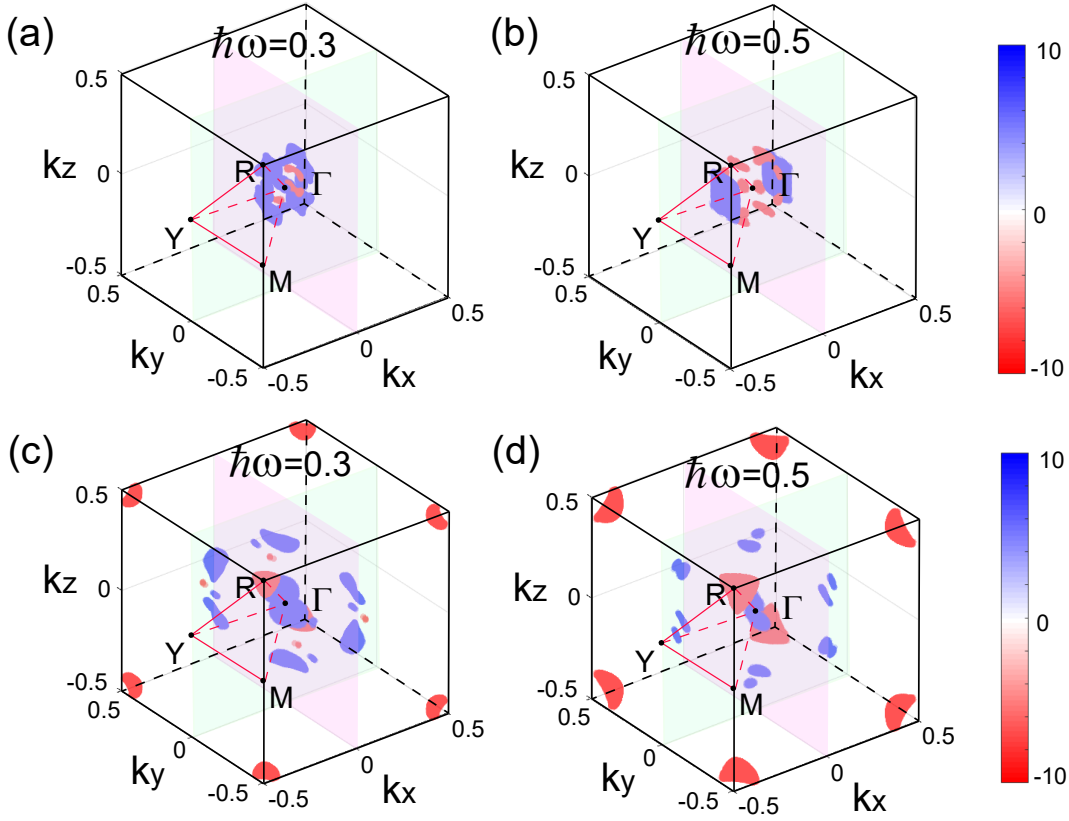


FIG. 2: (color online) (a)-(b) Momentum distribution of CPGE tensor β_{xx} from all bands without adjusting Fermi level at frequency $\hbar\omega = 0.3$ and 0.5 eV. (c)-(d) Momentum distribution of CPGE tensor β_{xx} in the Brillouin zone from all bands with Fermi level $E_f = E_{sixfold}$ at frequency $\hbar\omega = 0.3$ and 0.5 eV.

plaining that the quantization disappears in Fig.1(b), we take two frequencies as examples to calculate the local momentum distribution of CPGE tensor β_{xx} . When two degenerate points with opposite charge can simultaneously provide CPGE, the quantization will disappear and the total of CPGE is close to zero. Hence, two frequencies $\hbar\omega = 0.3$ and 0.5 eV are chosen, where only the fourfold degenerate point can contribute CPGE. From Fig.2(a)-(b), one can easily see that the trivial bands are mainly attributed to CPGE trace and the closed surface \vec{S} wrapping degenerate point also absent. As discussed in Section. III, the single multifold degenerate point with non-trivial topological charge can contribute to quantized CPGE trace in a certain frequency range, and the CPGE trace can be understood as the Berry curvature penetrating through closed surface \vec{S} wrapping degenerate point. The results in Fig.2(a)-(b) does not satisfy the conditions for obtaining quantized CPGE trace, and hence the quantization of CPGE trace with Fermi level lying at the charge neutral point can not be observed in our calculations.

To further explore the quantized CPGE trace in RhSi and provide clues for experimental research, we can dope holes and electrons in our calculations by reducing and raising the Fermi level. In doping holes the quantized CPGE trace is always absent, while the quantized platform close to $4\beta_0$ can be

acquired in a certain range in doping electrons. In the following, we will describe both cases in detail.

In doping holes in RhSi by reducing Fermi level, and the quantized platform is similar to that of Fermi level lying at the charge neutral points and always absent in a certain range of doping holes. We will analyze the reasons by focusing on the case of Fermi level at sixfold degeneracy. Fig.1(c) show the CPGE trace with Fermi level $E_f = E_{sixfold}$. Although the optical transitions near fourfold fermion are forbidden due to Pauli blocking in the frequency range from 0.1 to 0.5 eV, the plateau close to $4\beta_0$ contributed to sixfold degeneracy is absent. Similar to the no doping case, the CPGE trace provided by trivial bands can compete with that contributed by the sixfold degeneracy point. Fig.2(c)-(d) show momentum distribution of CPGE tensor β_{xx} in the Brillouin zone from all bands with Fermi level $E_f = E_{sixfold}$ at frequency $\hbar\omega = 0.3$ and 0.5 eV, and it is clear that the quantized CPGE trace is greatly affected by trivial bands, indicating that the quantization of CPGE trace disappears in doping holes.

In doping electrons, we focus on the Fermi level at fourfold degeneracy. A nearly plateau close to $4\beta_0$ with the frequency from 0.1 to 0.6 eV is shown in Fig.1(d), where in the frequency range only optical transitions near Γ can contribute to CPGE trace and the optically active fourfold fermion plays a

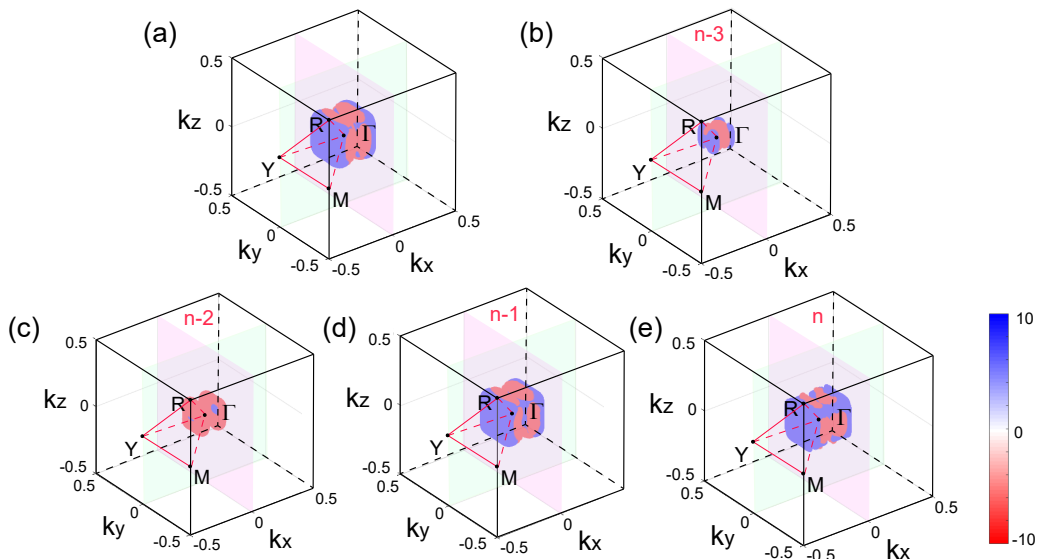


FIG. 3: (color online) Momentum distribution of CPGE tensor β_{xx} in the Brillouin zone at frequency $\hbar\omega = 0.5eV$ with corresponding Fermi level $E_f = E_{fourfold}$. (a) Momentum distribution from all bands with optically allowed transitions; (b)-(e) Momentum distribution from band-(n-3) to band-n, respectively.

major role. When optical frequency ω is more than 0.6 eV, the sixfold fermion can begin to provide CPGE trace, and cancel the contribution from fourfold fermion, indicating that the CPGE trace is close to zero from 0.7 to 2 eV. As discussed in Section. III, some contributions to CPGE from other bands can not rule out, and the exact quantization $4\beta_0$ range from 0.1 to 0.6 eV and exact zero range from 0.6 to 2 eV are absent in the DFT calculations. To analyze CPGE trace further, we calculate the momentum distribution of CPGE trace in the Brillouin zone in the above different frequency ranges. Firstly, Fig.3 show the momentum distribution of CPGE trace at frequency $\hbar\omega = 0.5eV$. Fig.3(a) displays momentum distributions from all bands with optically allowed transitions, indicating that the CPGE completely contribute to electric optical transitions of bands near Γ . Momentum distributions from the band-(n-3) to band-n are shown in Fig.3(b)-(e) respectively, where only the band-(n-2) and n are from fourfold fermion at Γ point and trivial band-(n-3) and n can provide small but finite CPGE trace shown in Fig.3(b) and (d), suggesting that the exact quantization $4\beta_0$ is absent. Secondly, Fig.4(a)-(f) show momentum distributions of CPGE trace in the Brillouin zone (BZ) from all bands with optically allowed transitions, where the frequency range is from $\hbar\omega = 0.7eV$ to $\hbar\omega = 1.8eV$. Range from 0.7 to 1.1 eV, the CPGE trace mainly contribute to electric optical transitions near Γ and R points shown in Fig.4(a)-(c). Fig.4(d)-(f) show the CPGE trace of frequency from 1.2 to 1.8 eV, which is provide from trivial band structures. Hence, the CPGE trace of frequency from 0.7 to 1.8 eV should close to zero.

Except for the Fermi level at fourfold degeneracy in doping electrons, we also calculate the trace of the CPGE tensor in other Fermi levels, shown in Fig.5(a)-(c). The Fermi level from 0.1 to 0.5 eV, the quantized platform close to $4\beta_0$ always

exists in a certain range, which opens up more possibility for experimentally observed quantized CPGE trace in RhSi.

Since there are other related compounds (CoSi, PdGa, PtGa, PtAl, RhSn) similar to RhSi in the experiment, we also calculate the CPGE trace of these compounds. Among these compounds, PtAl is also an alternative material for obtaining quantized CPGE. In doping electrons, a quantized CPGE trace can be obtained in a certain range with the Fermi level from 0.1 to 0.45 eV, shown in Fig.5(d)-(f).

V. CONCLUSION

In summary, circular photogalvanic effect (CPGE) of the topological semimetal with chiral multifold fermions were calculated based on realistic ab-initio band structures. We find that the quantized signal is very sensitive to the trivial bands away from high symmetry points. A nearly quantized value equal to the topological charge of chiral multifold fermions can be obtained by tiny doping. When the chemical potential is around from 0.1 to 0.5 eV, A plateau close to 4 exists in the frequency range. In addition to RhSi, PtAl is also an alternative material for obtaining quantized CPGE, which appears in a certain range.

VI. ACKNOWLEDGMENTS

This work was financially supported by the ERC Advanced Grant No. 291472 Idea Heusler, ERC Advanced Grant No. 742068 TOPMAT. This work was performed in part at the Center for Nanoscale Systems (CNS), a member of the National Nanotechnology Coordinated Infrastructure Network

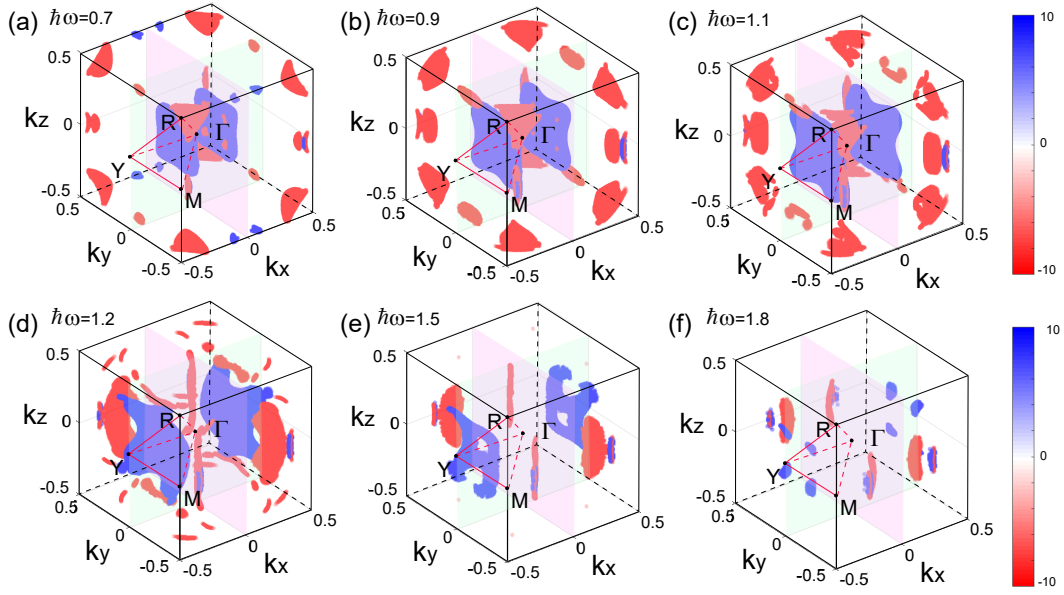


FIG. 4: (color online) Momentum distribution of CPGE tensor β_{xx} in the Brillouin zone from all bands with corresponding Fermi level $E_f = 0.077\text{eV}$. (a)-(f) The frequency range is from $\hbar\omega = 0.7\text{eV}$ to $\hbar\omega = 1.8\text{eV}$.

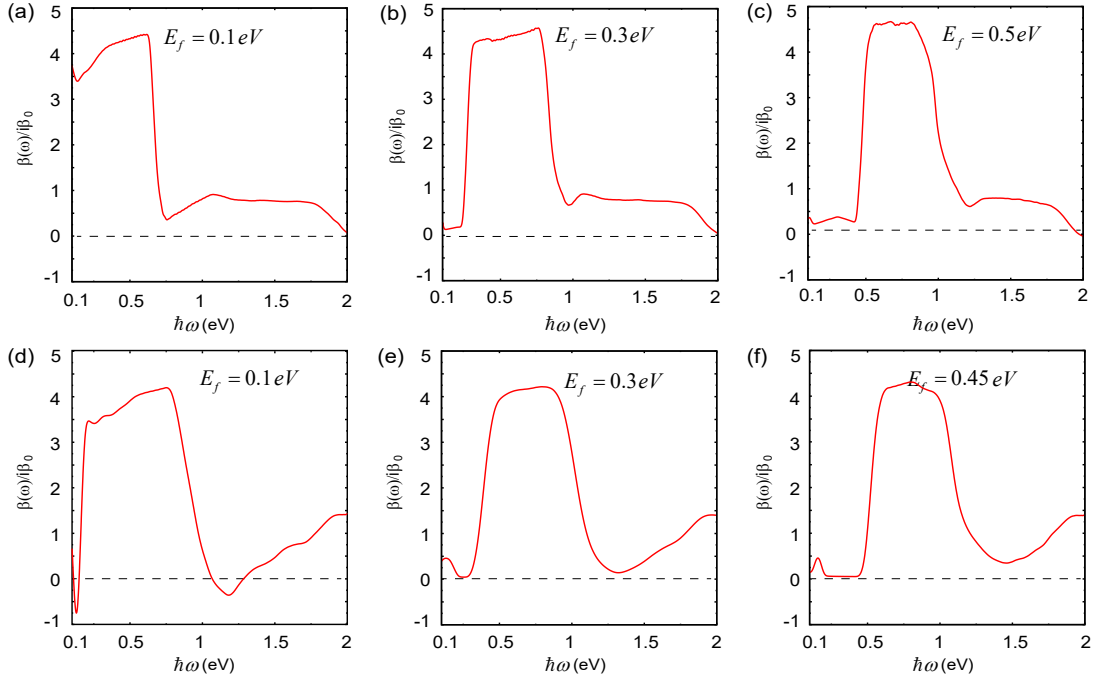


FIG. 5: (color online) The trace of the CPGE tensor as a function of frequency $\hbar\omega$ by DFT calculations with different Fermi levels (a)-(c) RhSi and (d)-(f) PtAl.

(NNCI), which is supported by the National Science Foundation under NSF award no. 1541959. CNS is part of Harvard

University. Some of our calculations were carried out on the Cobra cluster of MPCDF, Max Planck society.

* Electronic address: Corresponding: ysun@cpfs.mpg.de

¹ C.-K. Chiu, J. C. Y. Teo, A. P. Schnyder, and S. Ryu, Rev. Mod.

- Phys. **88**, 035005 (2016).
- ² N.P. Armitage, E. J. Mele, Ashvin Vishwanath, Rev. Mod. Phys. **90**,015001 (2018).
 - ³ Barry Bradlyn, Jennifer Cano, Zhijun Wang, M. G. Vergniory, C. Felser, R. J. Cava, B. Andrei Bernevig, Science 353, aaf5037 (2016)
 - ⁴ G. Xu, H. M. Weng, Z. J. Wang, X. Dai and Z. Fang, Phys. Rev. Lett. **107**, 186806 (2011).
 - ⁵ X. G. Wan, A. M. Turner, A. Vishwanath and S. Y. Savrasov, Phys. Rev. B **83**, 205101 (2011).
 - ⁶ Shuichi Murakami, New Journal of Physics **9**, 356 (2007).
 - ⁷ A. A. Burkov and L. Balents, Phys. Rev. Lett. **107**, 127205 (2011).
 - ⁸ S.-Y. Xu, I. Belopolski, N. Alidoust, M. Neupane, G. Bian, C. Zhang, R. Sankar, G. Chang, Z. Yuan, C.-C. Lee, S.-M. Huang, H. Zheng, J. Ma, D. S. Sanchez, B. Wang, A. Bansil, F. Chou, P. P. Shibayev, H. Lin, S. Jia, and M. Z. Hasan, Science **349**, 613 (2015).
 - ⁹ B. Q. Lv, N. Xu, H. Weng, J. Ma, P. Richard, X. Huang, L. Zhao, G. Chen, C. Matt, F. Bisti, V. Strocov, J. Mesot, Z. Fang, X. Dai, T. Qian, M. Shi, and H. Ding, Nature Phys. **11**, 724 (2015),
 - ¹⁰ B. Q. Lv, H. M. Weng, B. B. Fu, X. P. Wang, H. Miao, J. Ma, P. Richard, X. C. Huang, L. X. Zhao, G. F. Chen, Z. Fang, X. Dai, T. Qian, and H. Ding, Phys. Rev. X **5**, 031013 (2015).
 - ¹¹ C. Shekhar, A. K. Nayak, Y. Sun, M. Schmidt, M. Nicklas, I. Leermakers, U. Zeitler, Y. Skourski, J. Wosnitza, Z. Liu, Y. Chen, W. Schnelle, H. Borrmann, Y. Grin, C. Felser, and B. Yan, Nature Phys. **11**, 645 (2015).
 - ¹² L. X. Yang, Z. K. Liu, Y. Sun, H. Peng, H. F. Yang, T. Zhang, B. Zhou, Y. Zhang, Y. F. Guo, M. Rahn, D. Prabhakaran, Z. Hussain, S.-K. Mo, C. Felser, B. Yan, and Y. L. Chen, Nature Phys. **11**, 728 (2015)
 - ¹³ S.-Y. Xu, N. Alidoust, I. Belopolski, Z. Yuan, G. Bian, T.-R. Chang, H. Zheng, V. N. Strocov, D. S. Sanchez, G. Chang, C. Zhang, D. Mou, Y. Wu, L. Huang, C.-C. Lee, S.-M. Huang, B. Wang, A. Bansil, H.-T. Jeng, T. Neupert, A. Kaminski, H. Lin, S. Jia, and M. Zahid Hasan, Nature Phys. **11**, 748 (2015).
 - ¹⁴ S. M. Young, S. Zaheer, J. C. Y. Teo, C. L. Kane, E. J. Mele and A. M. Rappe, Phys. Rev. Lett. **108**, 140405 (2012).
 - ¹⁵ Z. J. Wang, Y. Sun, X. Q. Chen, C. Franchini, G. Xu, H. M. Weng, X. Dai and Z. Fang, Phys. Rev. B **85**, 195320 (2012).
 - ¹⁶ Z. J. Wang, H. M. Weng, Q. S. Wu, X. Dai and Z. Fang, Phys. Rev. B **88**, 125427 (2013).
 - ¹⁷ Congcong Le, Shengshan Qin, Xianxin Wu, Xia Dai, Peiyuan Fu, Chen Fang, and Jiangping Hu, Phys. Rev. B **96**, 115121 (2017).
 - ¹⁸ Congcong Le, Xianxin Wu, Shengshan Qin, Yinxiang Li, Ronny Thomale, Fu-Chun Zhang, and Jiangping Hu, Proceedings of the National Academy of Sciences 115, 8311 (2018).
 - ¹⁹ A. A. Soluyanov, D. Gresch, Z. J. Wang, Q. S. Wu, M. Troyer, X. Dai and B. A. Bernevig, Nature **527**, 495-498 (2015).
 - ²⁰ A. A. Burkov, J. Phys.: Condens. Matter **27**, 113201 (2015)
 - ²¹ E. V. Gorbar, V. A. Miransky, I. A. Shovkovy, Phys. Rev. B **89**, 085126 (2014).
 - ²² E. Liu, Y. Sun, N. Kumar, L. Muechler, A. Sun, L. Jiao, S.-Y. Yang, D. Liu, A. Liang, Q. Xu, et al., Nat. Phys. **14**, 1125 (2018).
 - ²³ Q. Wang, Y. Xu, R. Lou, Z. Liu, M. Li, Y. Huang, D. Shen, H. Weng, S. Wang, and H. Lei, Nat. Commun. **9**, 3681 (2018).
 - ²⁴ Y. Sun, Y. Zhang, C. Felser, and B. Yan, Phys. Rev. Lett. **117**, 146403 (2016).
 - ²⁵ S. Zhong, J. E. Moore, and I. Souza, Phys. Rev. Lett. **116**, 077201 (2016).
 - ²⁶ J. Ma and D. A. Pesin, Phys. Rev. B **92**, 235205 (2015).
 - ²⁷ C.-K. Chan, N. H. Lindner, G. Refael, and P. A. Lee, Phys. Rev. B **95**, 041104(R) (2017).
 - ²⁸ Q. Ma et al., Nat. Phys. **13**, 842 (2017).
 - ²⁹ F. de Juan, A. G. Grushin, T. Morimoto, and J. E. Moore, Nat. Commun. **8**, 15995 (2017).
 - ³⁰ Felix Flicker, Fernando de Juan, Barry Bradlyn, Takahiro Morimoto, Maia G. Vergniory, and Adolfo G. Grushin, Phys. Rev. B **98**, 155145 (2018).
 - ³¹ H. Nielsen and M. Ninomiya, Nuclear Physics B **193**, 173 (1981).
 - ³² H. Nielsen and M. Ninomiya, Nuclear Physics B **185**, 20 (1981).
 - ³³ H. Nielsen and M. Ninomiya, Physics Letters B **105**, 219 (1981).
 - ³⁴ Daniel S. Sanchez, Ilya Belopolski, Tyler A. Cochran, Xitong Xu, Jia-Xin Yin, Guoqing Chang, Weiwei Xie, Kaustuv Manna, Vicky Sub, Cheng-Yi Huang, Nasser Alidoust, Daniel Multer, Songtian S. Zhang, Nana Shumiya, Xirui Wang, Guang-Qiang Wang, Tay-Rong Chang, Claudia Felser, Su-Yang Xu, Shuang Jia, Hsin Lin, M. Zahid Hasan, Nature **567**, 500 (2019).
 - ³⁵ Guoqing Chang, Su-Yang Xu, Benjamin J. Wieder, Daniel S. Sanchez, Shin-Ming Huang, Ilya Belopolski, Tay-Rong Chang, Songtian Zhang, Arun Bansil, Hsin Lin, and M. Zahid Hasan, Phys. Rev. Lett. **119**, 206401 (2017).
 - ³⁶ P. Tang, Q. Zhou, S.-C. Zhang, Phys. Rev. Lett. **119**, 206402 (2017).
 - ³⁷ Dylan Rees, Kaustuv Manna, Baozhu Lu, Takahiro Morimoto, Horst Borrmann, Claudia Felser, J.E. Moore, Darius H. Torchinsky, J. Orenstein, arXiv:1902.03230v2 (2019)
 - ³⁸ J. E. Sipe and A. I. Shkrebtii, Phys. Rev. B **61**.5337 (2000)
 - ³⁹ J. R. Yates, X. Wang, D. Vanderbilt, and I. Souza, Phys. Rev. B **75**, 195121 (2007)
 - ⁴⁰ K. Koepnick and H. Eschrig, Phys. Rev. B **59**, 1743 (1999).
 - ⁴¹ J. P. Perdew, K. Burke, and M. Ernzerhof, Phys. Rev. Lett. **77**, 3865 (1996).